High-Resolution Phosphorus Nuclear Magnetic Resonance Spectra of Yeast Phenylalanine Transfer Ribonucleic Acid. Melting Curves and Relaxation Effects†

David G. Gorenstein* and Bruce A. Luxon

ABSTRACT: In a continuation of our studies on structural effects on the ^{31}P chemical shifts of nucleic acids, we present ^{31}P NMR spectra of yeast phenylalanine tRNA in the presence and absence of Mg^{2+}. Superconducting field (146 MHz) and 32-MHz ^{31}P NMR spectra reveal ~15 nonhelical diester signals spread over ~7 ppm besides the downfield terminal 3′-phosphate monoester. In the presence of 10 mM Mg^{2+}, most scattered and main cluster signals do not shift between 22–66 °C, thus supporting our earlier hypothesis that ^{31}P chemical shifts are sensitive to phosphate ester torsional and bond angles. At 70 °C, all of the signals merge into a single random coil conformation signal. Similar effects are observed in the absence of Mg^{2+} except that the transition melting temperature is ~20 °C lower. Measured spin–lattice and spin–spin relaxation times reveal another lower temperature transition besides the thermal denaturation process. A number of the scattered peaks are shifted (0.2–1.7 ppm) and broadened between 22 and 66 °C in the presence of Mg^{2+} as a result of this conformational transition between two intact tertiary structures. The loss of the scattered peaks in the absence of Mg^{2+} occurs in the temperature range expected for melting of a tertiary structure. An attempt to simulate the ^{31}P spectra of $tRNA^{Phe}$ based upon the X-ray crystallographically determined phosphate ester torsional angles supports the suggestion that the large shifts in the scattered peaks are due to bond angle distortions in the tertiary structure.

Gueron & Shulman (1975) have recently shown that the high-field ^{31}P NMR spectra of tRNA contain considerable fine structure. A number of individual phosphate resonances spread over ~6 ppm could even be resolved which were not revealed in earlier ^{31}P spectra at nonsuperconducting fields (Gueron, 1971; Weiner et al., 1974; Gorenstein & Kar, 1975).

We have proposed that ^{31}P chemical shifts of phosphate esters are sensitive to changes in O–P–O bond angles (Gorenstein, 1975) and ester torsional angles (Gorenstein & Kar, 1975; Gorenstein et al., 1976a; Gorenstein, 1977), and model system studies on single- and double-stranded nucleic acids (Gorenstein et al., 1976a; Gorenstein, 1978; D. G. Gorenstein and B. A. Luxon, unpublished experiments) suggest that a phosphate diester in a gauche,gauche (g,g) conformation should resonate upfield from a diester in a nongauche conformation. The ^{31}P NMR spectra of $tRNA^{Phe}$ should provide a good test of this prediction since a comparison with the known X-ray structure of yeast $tRNA^{Phe}$ (Jack et al., 1976; Quigley et al., 1975; Stout et al., 1978; Sussman et al., 1978) can be made. Both high-field and nonsuperconducting field ^{31}P NMR spectra of yeast $tRNA^{Phe}$ are reported, and a first effort at calculating the spectra is made, based upon the structural sensitivity to ^{31}P chemical shifts and the X-ray structure.

Experimental Section

Yeast $tRNA^{Phe}$ samples were prepared in a similar fashion to the method of Gueron & Shulman (1975). Freshly boiled buffers and sterile glassware, which had previously been leached for at least 1 h in 40% nitric acid, were used.

Dialysis tubing was boiled for 1 h in 5% $NaHCO_3$ and 2% EDTA and then twice more in H_2O for 1 h each to ensure the removal of divalent metal ions. The tRNA (20 mg) was dissolved in 4 mL of glass-redistilled water and dialyzed once or twice for 3 h at 4 °C against 0.5 L of buffer (0.1 M NaCl, 0.01 M cacodylate, and Mg^{2+} where indicated, pH 7.0) containing 10^{-2} M EDTA and then overnight at 4 °C against 1 L of buffer containing 10^{-3} M EDTA. The sample was concentrated on an Amicon high-pressure microfiltration cell by using a UM-2 filter to 0.5 mL. For the high-field NMR studies the tRNA solution plus 10% D_2O (reported buffer concentration is uncorrected for dilution) for field-locking was placed in a Wilmad spherical microcell which in turn was inserted into a 12-mm o.d. NMR tube containing the buffer. In the low-field NMR studies the sample was placed in a 5-mm NMR tube.

High-field, Fourier transform ^{31}P NMR spectra were taken on a Nicolet NTC-360 spectrometer (8.46 T) with proton noise decoupling, 90° pulses, 16K data points, and 1.86-s recycle time. At low field, 70° pulses, 8K data points, and 2.05-s recycle times were used. Sample temperature was regulated by a flow of nitrogen gas over the NMR tube. Unfortunately, the proton noise decoupling (4–5 W) on the superconducting spectrometer resulted in substantial heating of the sample and the temperature of the gas stream was not an accurate measure of the temperature of the microcell. An approximate correction of 21 °C was added to all of the gas stream measured temperatures on the high-field spectrometer. This correction was estimated by a comparison of the ^{31}P temperature-dependent NMR spectra of the same tRNA sample on NTC-360 and Bruker WP-80 (1.9 T) spectrometers. Heating is not a problem at lower fields with a 5-mm sample tube. In addition, this correction has been supported by new studies (not reported) in which we use a two-level decoupling procedure and surround the microcell with distilled water rather than with buffer. Heating at 146 MHz is reduced by this procedure. The same $tRNA^{Phe}$ sample (10 mM Mg^{2+}) was used for most of the temperature runs on the NTC-360 and WP-80 spec-

† From the Department of Chemistry, University of Illinois at Chicago Circle, Chicago, Illinois 60680. This is the second paper in a series (Gorenstein & Kar, 1975). Support of this research by the National Science Foundation (7707043) and the National Institute of Health (GM-17575) is gratefully acknowledged. D.G.G. is a fellow of the Alfred P. Sloan Foundation and the Fulbright Commission for the Exchange of Scholars. Use of the Purdue Biological Magnetic Resonance Laboratory supported by National Institutes of Health Grant No. RR01077 is acknowledged. The purchase of the WP-80 spectrometer was assisted by a National Science Foundation Departmental Equipment Grant.

0006-2960/79/0418-3796$01.00/0

trometers. At 146 MHz, the sample was heated in the sequence 34, 44, 49, 54, 60, and then 66 °C. At 32 MHz, the heating sequence was 22, 27, 31, 35, 40, 50, 60, and 22 again, 27 again, 35 again, 45, 55, 65, and then 70 °C. A different sample (10 mM Mg^{2+}) was used for the 70–83 °C runs. All tRNA spectral changes were reversible except that during the three cycles of heating and cooling (over ~6 days) there was a gradual increase in the 2′,3′-cyclic phosphate signal and additional phosphate monoester signals. Originally, 0–0.2 cyclic phosphate (relative to the 76 phosphates for the intact tRNA) was observed. At the beginning of the WP-80 run ~0.9 cyclic phosphate and 1.2 additional monoesters were apparent, increasing to a total impurity level of ~3 phosphates by the end of the run.

Chemical shifts are referenced to an external sample of 15% H_3PO_4 in D_2O at ambient temperature, which is 0.453 ppm upfield from 85% H_3PO_4 with external D_2O lock. Positive chemical shifts are downfield from phosphoric acid.

Spin–lattice relaxation times, T_1, were measured on the NTC-360 spectrometer by using an inversion-recovery pulse sequence $[[180° - \tau - 90°\ (\text{FID}) - T]_n$, where T = the wait time between pulse sequences, n = the number of scans, and τ = the variable delay time]. In this well-known pulse sequence T is usually set to about 5 times the longest T_1 expected (or longer) in order to ensure that the system has effectively recovered its equilibrium spin magnetization (hence maximum signal intensity). Systems such as the tRNA which require thousands of accumulations to achieve reasonable signal to noise ratios are almost prohibitively time consuming if the 5 $T_{1(max)}$ requirement is upheld. Fortunately, a fast inversion-recovery experiment (FIRFT) has been proposed by Canet et al. (1975) whereby the intersequence waiting time T is on the order of 1 $T_{1(max)}$. Time savings are significant for the FIRFT, possibly approaching an order of magnitude, with only a small reduction in dynamic range [essentially equivalent to sensitivity for a set of T_1 spectra (Freeman & Hill, 1971)]. Further time was saved by using the Nicolet-supplied three-parameter T_1 fit program T131R which obviated the need to obtain a spectrum with τ in excess of 5 $T_{1(max)}$. Generally this is necessary to assign the signal intensity at thermal equilibrium, S_0. Levy & Peat (1975) have shown, however, that at T/T_1 ratios of less than 3 the apparent S_0 can deviate significantly from the "true" equilibrium S_0, introducing significant error in S_τ for long τ and hence poor calculated values for T_1. The Nicolet program, however, performs a three-parameter fit to eq 1, where W = –(amplitude

$$y = S_0*[1 - [1 + W*[1 - \exp(-T/T_1)]]* \exp(-\tau/T_1)] \quad (1)$$

of S_τ at $\tau = 0$). The exponential fit [as suggested by Levy & Peat (1975)] calculates a "best" value for S_0, saving the time otherwise required to run the experiment with $\tau \geq 5$ $T_{1(max)}$.

To minimize heating of the sample from the decoupler, the decoupler was gated low (45 dB, 1 W) at all times except during collection of the FID when it was gated high (48 dB, 5 W).

Results

The temperature dependence of the ^{31}P chemical shifts of yeast tRNA^{Phe} in 0.1 M NaCl and 10 mM Mg^{2+} is shown in Figure 1. The 146-MHz spectrum at 34 °C is similar to that reported by Gueron & Shulman (1975) under similar conditions at 109 MHz. Clustered around –1 ppm are the main resonances of the backbone phosphates. At +3.4 ppm is the 3′-terminal phosphate (integrating for 1/76 of the total

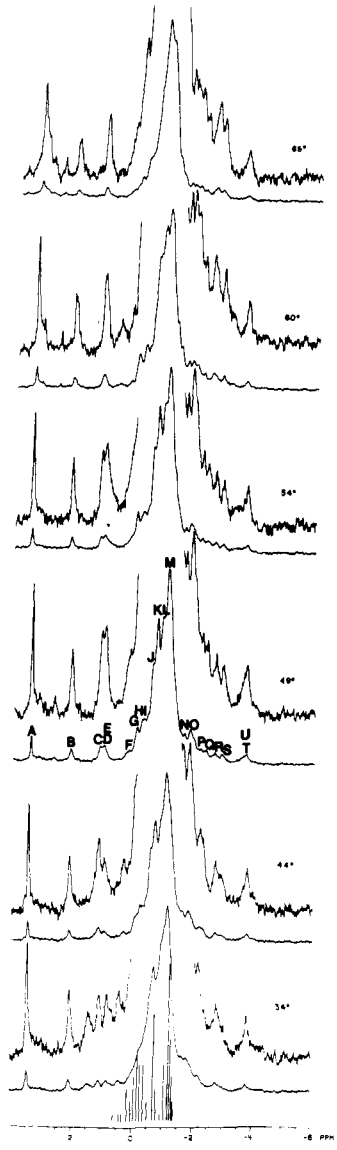

FIGURE 1: ^{31}P NMR spectra of yeast phenylalanine tRNA (~33 mg/mL) in 100 mM NaCl, 10 mM cacodylate, 10 mM $MgCl_2$, 1 mM EDTA, and 10% D_2O, pH 7.0, at indicated temperatures (°C). The expanded scale for the scattered peaks is shown over the normal spectrum. A simulated stick figure spectrum is also shown at the bottom. Number of acquisitions, 8000 FID's, 1.86-s acquisition, 145.76 MHz. Chemical shifts are in parts per million from 15% H_3PO_4.

phosphate). In addition, upfield and downfield of the main cluster are ~15 scattered peaks, a number of which are well resolved. The temperature dependence of the chemical shifts of the resolvable scattered and main-cluster peaks is shown in Figure 2. In contrast to previous reported temperature-dependent ^{31}P chemical shifts of single- and double-stranded nucleic acids (Gorenstein et al., 1976a; Gorenstein, 1978), most of the peaks shift less than 0.2 ppm from 22 to 66 °C. Thus, over this temperature range the ^{31}P signal of a 1:1 poly-(A)/oligo(U) double helix shifts ~1.0 ppm downfield (D. G. Gorenstein and B. A. Luxon, unpublished experiments). This was suggested to arise from a melting of the double-stranded RNA with a –g,–g phosphate ester conformation to a mixture of random coil, single-stranded RNA with a mix of –g,–g plus non-g,g ester conformations. Previously (Gorenstein et al., 1976a), the ^{31}P signal of only a relatively rigid, conformationally restricted 2′,3′-cyclic cytidine monophosphate model compound was found to be temperature independent. The temperature insensitivity to most features in the tRNA ^{31}P

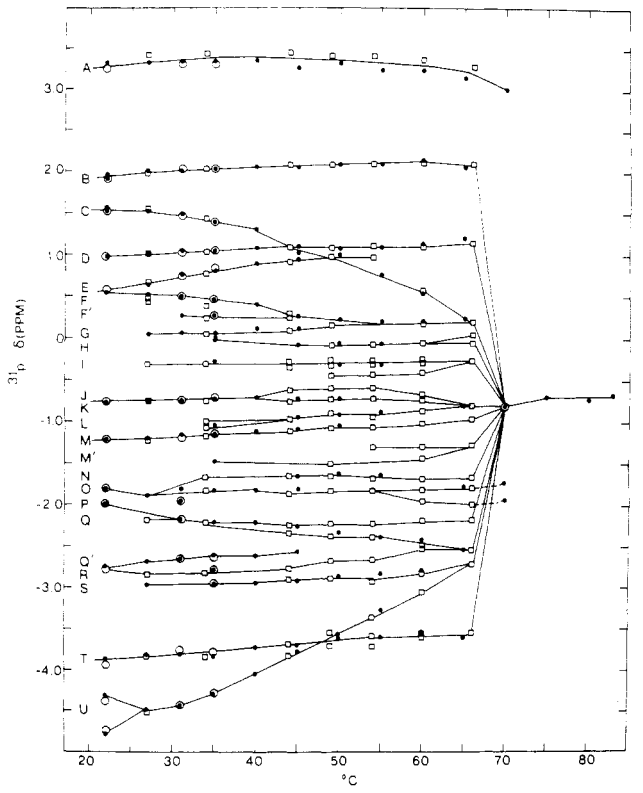

FIGURE 2: Temperature dependence of the chemical shifts, δ, of the peaks identified in Figure 1 for tRNA^{Phe} in 10 mM Mg^{2+} buffer: (□) 145.8 MHz, from spectra in Figure 1; (●) 32.37 MHz; (○) repeat spectra at 32.37 MHz.

Table I: Spin-Lattice Relaxation Times for tRNA^{Phe} [a]

peak	T_1 [b]	peak	T_1 [b]
A	2.54 (0.15)	M	2.50 (0.005)
B	3.50 (0.15)	N/O	2.09 (0.02)
C	2.86 (0.10)	P/Q	2.67 (0.14)
D	2.81 (0.18)	R	2.29 (0.05)
E	2.57 (0.16)	S	2.31 (0.13)
F	2.80 (0.14)	T	2.51 (0.35)
K	2.30 (0.03)		

[a] At 146 MHz, 27 °C, in 10 mM Mg^{2+} buffer. [b] Number in parentheses is the standard deviation.

spectrum in 10 mM Mg^{2+} suggests that the tRNA (and the backbone phosphates) retains its conformation throughout this temperature range and that little melting occurs in high Mg^{2+} concentration samples up to 66 °C.

In contrast to these modest changes in the ^{31}P spectra of the 10 mM Mg^{2+} tRNA sample, in the absence of Mg^{2+} the tRNA spectra change dramatically from 36 to 60 °C (Figures 3 and 4). The main upfield signals L′ and M at −1.0 ppm shift downfield by a total of 0.8–0.9 ppm with increasing temperature. The other main signals J + K at −0.5 ppm also shift downfield, and the two peaks merge at 70 °C. The shoulder peaks in the main cluster and all of the scattered peaks eventually lose intensity and merge into a single random coil diester peak at 40–50 °C. Similar spectral changes for tRNA^{Phe} in the absence of Mg^{2+} were reported by Gueron & Shulman (1975).

Relaxation Times. Spin–lattice relaxation times for the phosphates as determined from inversion-recovery FT spectra are reported in Table I. The T_1 values and the estimated errors are probably quite accurate for at least the two main signals K and M. The T_1 values for these two signals are little affected by changing phase settings. The T_1 values for the scattered peaks are, however, sensitive to the phase settings,

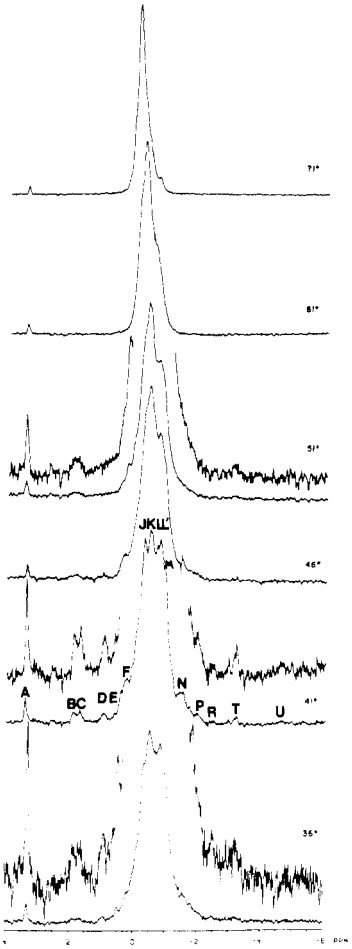

FIGURE 3: ^{31}P NMR spectra (145.8 MHz) of tRNA^{Phe} (33 mg/mL) in 100 mM NaCl, 10 mM cacodylate, 1 mM EDTA, no Mg^{2+}, and 10% D_2O, pH 7.0, at indicated temperatures (°C).

particularly the broader, poorly resolved signals that partially overlap with the base line of the main cluster signals. The significance of the difference in the T_1 values for the scattered peaks is thus questionable. More confidence can be placed on the T_1 values for peaks A–E, K, and M.

Previous studies have demonstrated that chemical shift anisotropy and proton dipolar interactions dominate the spin–lattice relaxation times of phosphates in the absence of paramagnetic metal ions (Hayashi et al., 1977; Gueron & Shulman, 1975; Berden et al., 1974). On the assumption of these two mechanisms, the phosphorus relaxation rate may be calculated from eq 2

$$\frac{1}{T_1} = A\left[\frac{\tau_c}{10}\left(\frac{3}{1+\omega_P^2\tau_c^2} + \frac{1}{1+(\omega_P-\omega_H)^2\tau_c^2} + \frac{6}{1+(\omega_P+\omega_H)^2\tau_c^2}\right)\right] + B\left(\frac{\tau_c}{1+\omega_P^2\tau_c^2}\right) \quad (2)$$

where

$$A = \sum_{i=1}^{n}(\gamma_P^2\gamma_H^2\hbar^2)/r_i^6$$

$$B = (2/15)\delta^2\omega_P^2$$

τ_c is the rotational correlation time, ω_P and ω_H are the Larmor angular frequencies of phosphorus and hydrogen, respectively, γ is the magnetogyric ratio, r_i is the distance between phosphorus and the ith proton, and δ is the chemical shift anisotropy (Abragam, 1961).

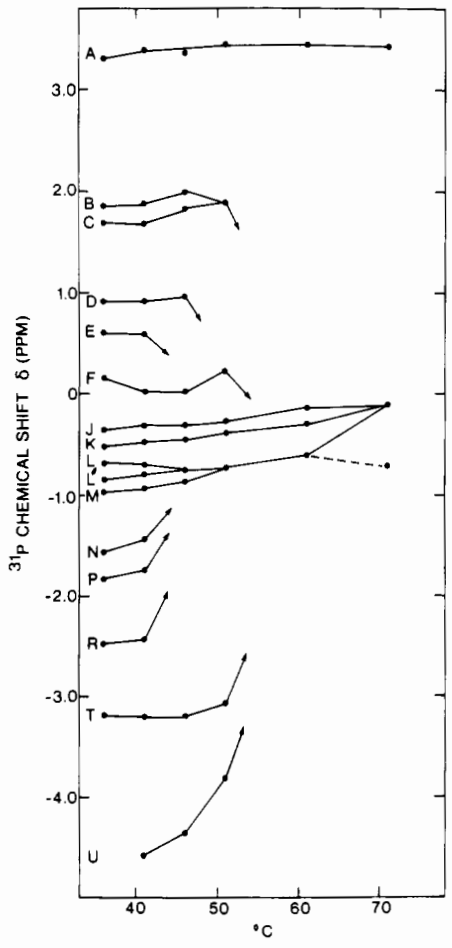

FIGURE 4: Temperature dependence of the chemical shifts, δ, of the indicated peaks from Figure 3 (in buffer without Mg^{2+}) at 145.8 MHz.

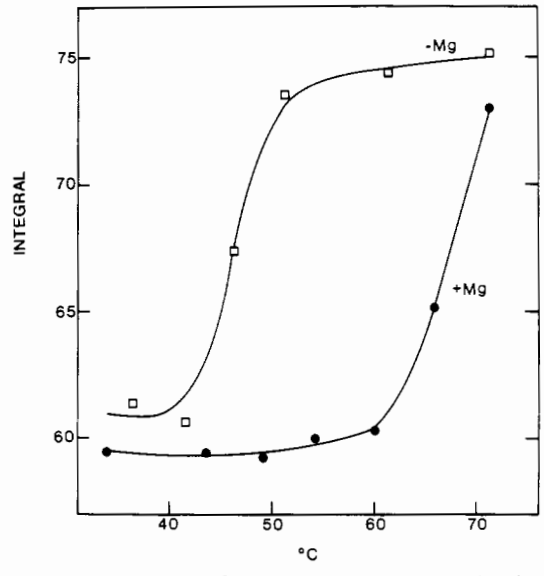

FIGURE 5: Melting curve for the total main cluster (peaks J–M) integrated intensity in the absence of Mg^{2+} (□) or in the presence of 10 mM Mg^{2+} (●) for tRNA^{Phe} at 145.8 MHz. Total intensity, 76 phosphates.

Relaxation at 146 Mhz is likely dominated by the chemical shift anisotropy mechanism (Berden et al., 1974; second term in eq 2). Application of the values for δ, r_i, and τ_c determined by Hayashi et al. (1977) at 40.48 MHz to our data at 146 MHz suggests that >90% of the spin–lattice relaxation comes from the chemical shift anisotropy term. This is also supported by the magnetic field strength dependence of the line widths

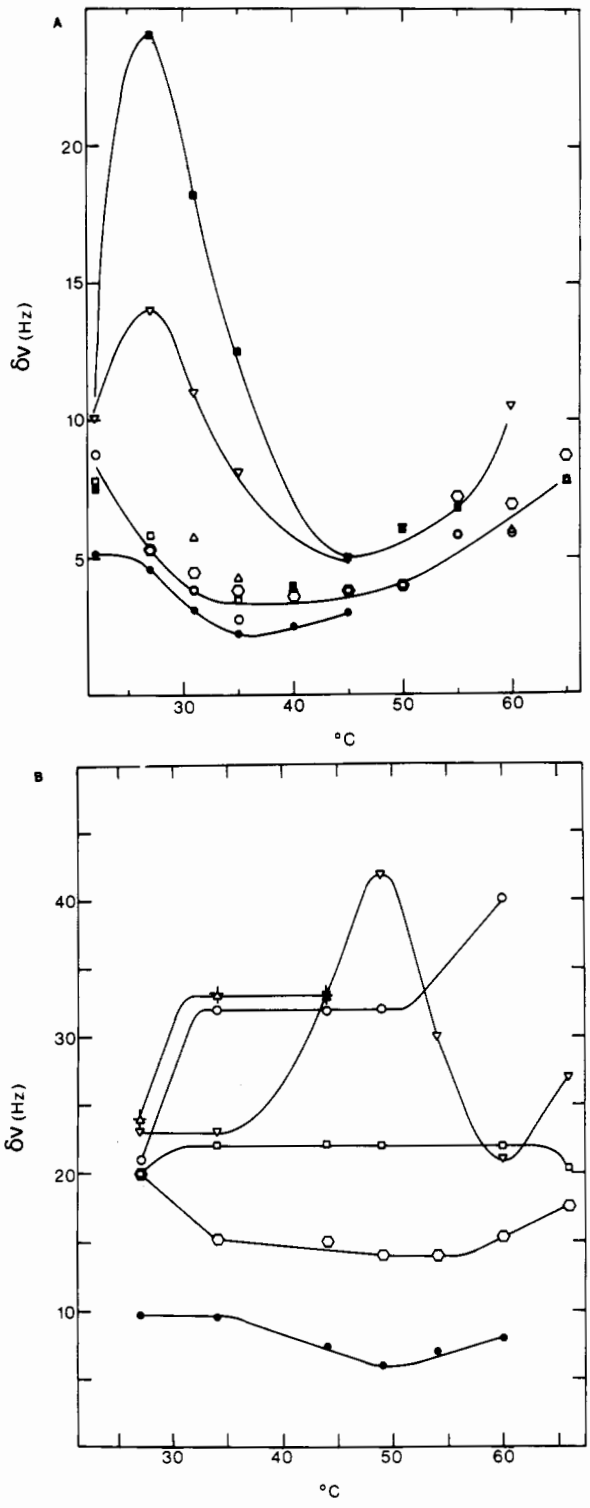

FIGURE 6: Plot of the corrected line widths at half-height, $\delta\nu$, for scattered peaks vs. temperature at 32.4 (A) and 145.8 MHz (B) for tRNA^{Phe} in 10 mM Mg^{2+} buffer for peaks A (●), B (□), C (○), D (□), E (△), F (+), T (▽), and U (■).

at half-height. Gueron & Shulman (1975) noted that the line width for the scattered peaks increased from 3 Hz at 40 Mhz to 14 Hz at 108 MHz. After being corrected for the instrumental line broadening, the line widths at 32 and 146 MHz are plotted in Figure 6 as a function of temperature. When the temperature dependence of the line widths, which as discussed below is due to chemical exchange effects, is discounted, the scattered peaks B–E have a minimum line width of 3–4 Hz at 32 MHz. At 146 MHz, peaks B–F have a ~20-Hz line width at 27 °C.

Assuming dominance of the chemical shift anisotropy mechanism, we can compute the spin–spin relaxation time, T_2, by eq 3 (Abragam, 1961). If the chemical shift an-

$$1/T_2 = (1/20)\omega^2\delta^2[4\tau_c + 3\tau_c/(1 + \omega^2\tau_c^2)] \quad (3)$$

isotropy mechanism dominates both the spin–lattice and spin–spin relaxation times at 146 MHz, we can unambiguously calculate a unique set of δ and τ_c from eq 2 and 3 and the measured T_1 and T_2 values. By use of these two equations in two unknowns, $\delta = 180 \pm 20$ ppm and $\tau_c = (1.1 \pm 0.2) \times 10^{-8}$ s. These values differ from those of Hayashi et al. (1977) for δ (120–130 ppm) and τ_c (5×10^{-9} s) but agree better with the τ_c of $(3 \pm 1) \times 10^{-8}$ s for the ribose carbons determined by Komoroski & Allerhand (1972) in a ^{13}C NMR relaxation study on yeast tRNA^{Phe}. The calculated line widths at 146, 109, 40, and 32 MHz are 19, 11, 1.6, and 1.1 Hz, respectively, assuming only a chemical shift anisotropy mechanism and our values for τ_c and δ. The dipole–dipole and other relaxation mechanisms presumably account for the difference (2–3 Hz) between the above calculated and observed line widths. Note that some alteration in Hayashi et al.'s reported δ and τ_c is required since the computed line width at 146 MHz using their data would only be ~5 Hz.

Calculated Phosphorus-31 Spectra. Gorenstein & Kar (1975) have calculated the ^{31}P chemical shifts for a phosphate diester in various conformations. Using CNDO/2 SCF MO methods, we drew a correlation between calculated phosphorus electron densities and ^{31}P chemical shifts. At that time a good model for an acyclic phosphate diester in various conformations did not exist, and the correlation was based upon observed and calculated shifts for various cyclic diesters. Since ^{31}P chemical shifts are also sensitive to O–P–O bond angles and cyclic esters have considerable bond angle as well as torsional angle variation (Gorenstein, 1975, 1977), the initial correlation was necessarily subject to some reservations. Potentially the X-ray structure and ^{31}P spectrum of yeast tRNA^{Phe} can provide a much better model to establish limits on the variation in ^{31}P chemical shifts due to torsional effects. Certainly a large number of the phosphates are in nonhelical conformations (Sussman et al., 1978) which would explain the large spread in the ^{31}P chemical shifts.

Earlier model studies on single-helical and double-helical polynucleotides have demonstrated that phosphate diesters in a gauche,gauche (g,g) conformation[1] are at least 1.0 ppm upfield of more open (such as gauche,trans or g,t) conformations (Gorenstein et al., 1976a; Gorenstein & Kar, 1975; Gorenstein, 1978; Patel & Canuel, 1976). The helical conformation commonly is g,g, and as suggested earlier (Gueron & Shulman, 1975; Gorenstein & Kar, 1975) the main upfield signal M at −1.2 ppm in the tRNA^{Phe} spectrum is likely associated with phosphates in this conformation.

Assuming that the ^{31}P signal of a phosphate ester in a g,t-type conformation is shifted 1.4 ppm downfield from a g,g phosphate, we can derive the relationship shown in eq 4, where

$$\delta_{calcd}(ppm) = -155.56P_A - 59.03 \quad (4)$$

P_A is the calculated (using the CNDO SCF MO method) charge density on phosphorus and is +0.3718 for a model g,g dimethyl phosphate and is +0.3808 for a g,t-type ester [see Gorenstein & Kar (1975)].

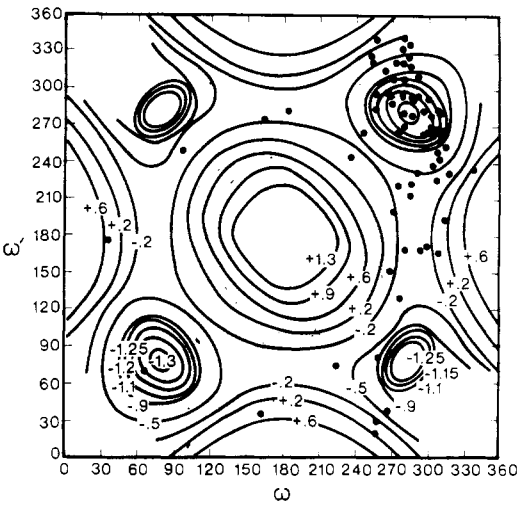

FIGURE 7: ^{31}P chemical shift–torsional angle contour map for a phosphate diester as calculated from eq 4. "Isoshift" contours are in parts per million from 15% H_3PO_4. Points (●) represent ester torsional angles ω and ω' from the Sussman et al. (1978) X-ray model for tRNA^{Phe}.

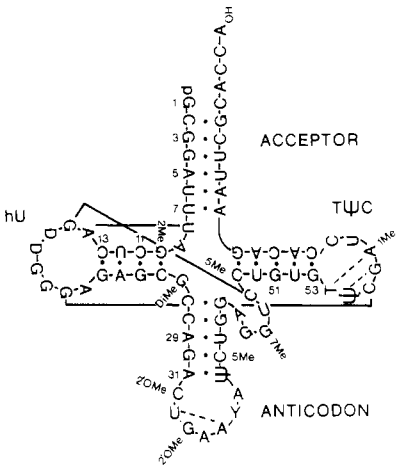

FIGURE 8: Cloverleaf model showing secondary and tertiary interactions in tRNA^{Phe}.

Carrying out MO charge density calculations on dimethyl phosphates possessing other torsional geometries, we can predict their ^{31}P chemical shifts based upon the correlation of eq 4 and then calculate a "chemical shift" contour map as shown in Figure 7. It is essential to emphasize that because of the limited knowledge of the true torsional variation of ^{31}P shifts and the known inadequacies of CNDO charge densities and linear chemical shift correlations such as eq 4, the possible errors in such a map may be substantial. At the very least, however, it is likely that relative shifts and limits may be reasonably obtained from this diagram.

A test of the validity of this map would be the degree to which it correctly simulates the ^{31}P spectrum of tRNA^{Phe}. The torsional angles ω and ω' for the 75 phosphate diesters from the X-ray structure of Sussman et al. (1978) are superimposed upon this map, and the simulated stick figure spectrum is shown under the actual spectrum in Figure 1. Although the central cluster shape is approximately reproduced in the computed spectrum, the fit to the scattered peaks is hopelessly inadequate. In the main cluster, the helical g,g phosphate peaks L and M between −0.9 and −1.5 ppm integrate for ~35

[1] The conformation of a diester is determined by the two dihedral angles ω and ω' defined by rotation about the phosphate ester bonds, RO–POR. For $\omega = \omega' = 0°$, the phosphate is in a cis, eclipsed conformation. For a dinucleoside monophosphate, ω is the conformation about the 3′-O–P bond and ω' is the conformation about the 5′-O–P bond. The angles are defined by a counterclockwise rotation (Sundaralingam, 1969). Note for a symmetrical dialkyl phosphate that the g,g and −g,−g conformations are identical.

phosphates while the X-ray structure indicates that there should be 32 phosphates that would have ^{31}P signals falling within this chemical shift range. Note that most but certainly not all of these phosphates correspond to the base-pair double-helical phosphates in the stems of the cloverleaf model (Figure 8). Surprisingly, in Sussman et al.'s refined X-ray structure, a number of these double-helical phosphates are apparently in non(-g,-g) conformations. Peaks J and K between -0.5 and -0.9 ppm integrate for ~16 phosphates and in the computed spectrum there are 14. Between +0.3 and -0.5 ppm (peaks F-I) there are only 8-9 phosphates while 26 are computed. Below 0.3 ppm, the integrated intensity of peaks B-E is 4 while 3 are computed (although the predicted chemical shifts are very much in error). Even worse, between -1.5 and -5 ppm there are 10-11 phosphates (peaks N-U) and *none* are predicted. There are several explanations for the failure to adequately account for these scattered peaks. First, it is certainly possible that a linear correlation between computed charge densities (the values themselves subject to question) and chemical shifts does not exist. However, similar treatment of other nonhydrogen nuclei has been shown to yield satisfactory correlations (Velenik & Lynden-Bell, 1970; Levy & Nelson, 1972). Another possible explanation for the poor fit of the computed spectra is the inadequacy of the X-ray crystal structure. In fact, there is a large variation in the phosphate ester torsional angles of tRNA in the X-ray models reported by various groups (Quigley et al., 1975; Sussman et al., 1978; Stout et al., 1978; Jack et al., 1976). This is a severe problem, and until a concensus on the torsional angles for the phosphates can be agreed upon by all groups, attempts to assign individual phosphates from the X-ray structure and a computed chemical shift will be impossible.

If the map of Figure 7 is at least qualitatively correct, then conformational effects are responsible for at most a spread of 2.6 ppm (g,g relative to t,t). This range is consistent with model system studies (Gorenstein, 1978; Gorenstein et al., 1976a). Since the actual spread in the scattered peaks is nearly 7 ppm, it would appear as though some factor other than torsional effects was responsible for the additional spread. It is quite likely that this second effect is ester RO-P-OR bond angle changes. We have previously noted that a reduction of ester O-P-O bond angles by ~10° results in a downfield shift of 20-30 ppm [Gorenstein, 1975, 1978; see also Blackburn et al. (1971)]. A large number of phosphate triesters, diesters, and monoesters are roughly linearly correlated to O-P-O bond angles so that a 2-3-ppm shift per degree of bond angle distortion might be expected from this correlation. Alteration of the ester bond angle through the tertiary interactions in the tRNA could readily explain the scattered peak shifts. The scattered downfield peaks would represent phosphates with bond angles several degrees smaller than normal, while the scattered upfield peaks would represent phosphates with bond angles several degrees larger than normal [note that O-P-O bond angles are normally strongly coupled to the ester conformation; see Gorenstein & Kar (1975) and Gorenstein (1977, 1978)]. Unfortunately, these bond angle differences are beyond the resolution of the present X-ray diffraction studies.

Discussion

Structural Interpretation of tRNA^{Phe} in the Presence of Mg^{2+}. Previous optical (Sprinzel et al., 1974) and ^1H NMR studies (Bolton & Kearns, 1977; Crothers et al., 1974; Davanloo-Malherbe et al., 1978; Kan et al., 1977; Robillard et al., 1977) have established that tRNA^{Phe} retains its tertiary and secondary structures up to 65-70 °C in the presence of 10 mM Mg^{2+}. The overall constancy of the ^{31}P spectra in the temperature range 22-66 °C is consistent with this conclusion, although some conformational changes are detected by ^{31}P NMR in this range. As shown in Figures 1 and 2, some of the scattered peaks show moderate upfield or downfield shifts with temperature. In addition, line broadening effects and analysis of the integrated intensities of the main cluster and scattered peaks suggest that a second lower temperature transition may be monitored with ^{31}P spectral changes.

The simplest model to analyze these results is in terms of a low-temperature (<50 °C) and high-temperature (>60 °C) transition. We suggest that transition I at lower temperatures is associated with the interconversion of two different conformations, both of which retain the main features of the secondary and tertiary structures found in the X-ray structure. Transition II at higher temperature represents the cooperative melting of the secondary and tertiary structures into a random coil.

Looking first at transition II, the spectral changes suggestive of thermal denaturation can be summarized as follows. As shown in Figure 6, the scattered signals B-F and T-U start broadening at ~50 °C (except for D at 146 MHz). Intensity changes are also observed for the well-resolved scattered peaks B-E, T, and U. At lower temperature peaks C + D + E integrate for three phosphates, and upon raising the temperature to 66 °C 1.5-2 phosphates are lost in the spectral region 0.4-1.5 ppm. Similarly, the upfield signals T + U, which integrate for a total of 2 phosphates at low temperature, integrate for only ~0.5 phosphate by 66 °C. Three more phosphates are lost in the spectral window encompassing peaks N-S by 66 °C.

Except for C and U, only small changes in the chemical shifts of the signals are observed between 50 and 60 °C. Suddenly, between 60 and 70 °C almost all of the scattered peaks disappear and the integrated intensity of the main cluster (J-M) increases to 73 phosphates (Figure 5). Only peaks N and O (integrating for 2 phosphates) and the terminal 3′-phosphate remain. Peaks N and O are g,g-type phosphates and suggest that some double-helical stem phosphates in one of the hairpin loops have not completely melted by 70 °C. At temperatures greater than 70 °C, all of the diester peaks merge into a single signal.

The broadening and intensity changes and lack of major chemical shift effects with temperature between 50 and 66 °C are consistent with slow chemical exchange[2] (Pople et al., 1959) between the native structure and the random coil. The chemical shift of the random coil is similar to that of peaks G-J, and as the population of the denatured random coil conformation increases between 60 and 70 °C, the signal intensities for the native structure are transferred into this region. By 66 °C, a total of ~6 phosphates out of the 16 scattered phosphates in the native structure are lost, representing ~36% in the melted state by 66 °C. The estimated melting temperature, $T_m \approx 68$ °C, from Figure 5 agrees with the single cooperative thermal transition between 65 and 75 °C estimated by optical and proton NMR techniques under similar conditions (Romer et al., 1970; Robillard et al., 1977).

In contrast to the slow chemical exchange observed for the thermal denaturation, transition II, the ^{31}P spectral changes for the lower temperature transition I are consistent with more rapid chemical exchange between two (or possibly more)

[2] On the NMR time scale, two signals are in slow exchange if $1/\tau \ll 2(\Delta\nu)$, where $\Delta\nu$ is the chemical shift difference between the two sites and τ is the lifetime of the state. For fast exchange, where only one averaged NMR signal is observed, $1/\tau \gg 2\pi(\Delta\nu)$.

different tertiary conformations.

While the downfield scattered peaks A, E′, H, and I show very little shift (<0.1 ppm) between 22 and 60 °C, the other peaks experience both upfield and downfield shifts. Peaks B, D, E, and G are shifted (+0.15, +0.15, +0.5, and +0.15 ppm, respectively) to lower field in the high-temperature "native" conformation. Peaks C and F are shifted (−0.9 and −0.3 ppm, respectively) upfield at higher temperature. Since many of the signals are not shifted in the direction of the denatured state (temperatures greater than 66 °C), it appears as though the high-temperature conformation in transition I retains full secondary and tertiary structure.

For the upfield scattered peaks, while N shows little shift with increasing temperature in transition I, others show upfield shifts, O (Δ = −0.1 ppm) and P (Δ = −0.5 ppm), and the rest downfield shifts, R (Δ = +0.3 ppm), S (Δ = +0.2 ppm), T (Δ = +0.3 ppm), and U (Δ = +1.7 ppm). The line widths for the resolvable peaks, especially T and U, are similarly temperature sensitive. At 32 MHz, the line width of peak T increases from 10 to 14 Hz and U increases from 8 to 24 Hz between 22 and 30 °C (Figure 6). With further increase in temperature, both signals resharpen to line widths of 5 Hz by ~45 °C (at 32 MHz). At superconducting fields, the line width for T increases from 22 Hz at 30 °C to 42 Hz at 49 °C. At 146 MHz, U broadens from ~70 Hz at 27 °C to 100 Hz at higher temperatures.

The line-broadening maximum with temperature for T and U and the frequency dependence of the line broadening are strong evidence for chemical exchange effects in transition I. The slow exchange broadening component of the line width, $\delta\nu_{ex}$, relates to the lifetime, τ_I, of the signal in this transition, with $1/\tau_I = \pi(\delta\nu_{ex})$, where $\delta\nu_{ex} = \delta\nu_{obsd} - \delta\nu_0$ and $\delta\nu_{obsd}$ is the observed line width and $\delta\nu_0$ is the intrinsic line width in the absence of chemical exchange (Pople et al., 1959). $\delta\nu_0$ can be estimated from the line width of signals B–E which show no evidence of any chemical exchange broadening (at least at 32 MHz and 35–50 °C), and thus for T at 30 °C: $\delta\nu_{ex} \approx 14 - 5 = 9$ Hz or $\tau_I \approx 35$ ms. For U, τ_I is estimated at 8 ms.

The lifetime can also be estimated from the chemical shift difference between the two sites, $\Delta\nu$: $\tau_I \approx \sqrt{2}/2\pi(\Delta\nu)$. This expression is only valid in the intermediate exchange region (where maximum line broadening occurs). With a chemical shift difference between the two conformations for the T peak of 0.3 ppm, τ_I is estimated at 23 ms, in reasonable agreement with the 35-ms lifetime at lower temperature in the slow exchange region. Because of the field dependence of $\Delta\nu$, at 146 MHz maximum broadening would occur at a rate of exchange ~4.5 times faster than at 32 MHz (146:32), or $\tau_I \approx 5$ ms. As shown in Figure 6, maximum broadening for peak T occurs 20 °C higher at 146 MHz than at 32 MHz. This temperature dependence is consistent with a factor of ~2 increase in rate of exchange per 10 °C rise in temperature for a transition with a "moderate" activation energy. Also, the line width at maximum broadening is larger at higher field strength. (For T and U, 14 and 24 Hz at 32 MHz, respectively, and 42 and >100 Hz at 146 MHz.)

The decrease in line widths for peaks B–E at 32 MHz from 22 to 36 °C is also likely an exchange broadening effect. The *increase* in line width for C–F at 146 MHz from 27 to 36 °C is certainly consistent with this suggestion since we again expect a field dependence to the chemical exchange broadening effect as described above. Below 36 °C and at 32 MHz these signals experience fast exchange while at 146 MHz they are in slow exchange. The minimum 12–13-Hz exchange broadening for C–F at 34 °C indicates $\tau_I \approx 24$ ms, consistent with the relaxation lifetime measured from line broadening of T. The anomalously small line width for B and its uniquely slow spin–lattice relaxation rate suggest that B is in a special environment.

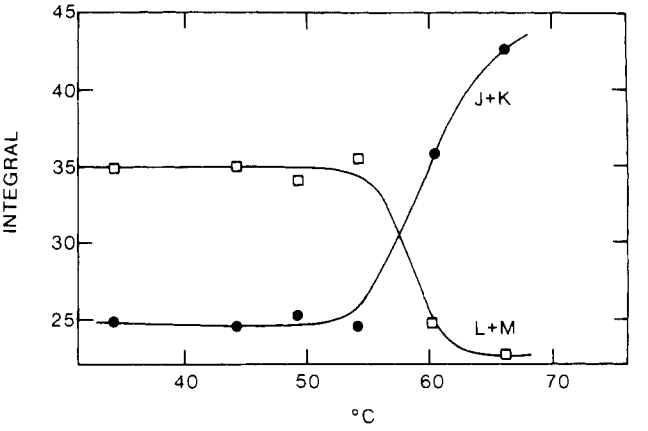

FIGURE 9: Plot of the integrated intensity for the helical (L + M, □) and nonhelical peaks (J + K, ●) in the main cluster for $tRNA^{Phe}$ in 10 mM Mg^{2+}, 145.8 MHz.

The estimated millisecond time scale for exchange cannot be due to a helix to coil transition since for hairpin loops lifetimes of 10–100 μ are expected (Cole & Crothers, 1972; no Mg^{2+} in 30 mM Na^+). Romer et al. (1970) and Coutts et al. (1975) have shown that disruption of the tertiary structure is associated with a longer (2–23 ms) relaxation time. It is possible that transition I represents interconversion between two different but complete tertiary structures and that exchange requires breaking and re-formation of tertiary structure.

While little observable change in the total intensity of the main cluster peaks is noted below 60 °C, the distribution of the phosphates in the downfield cluster (J + K) and the upfield cluster (L + M) alters sharply around 58–61 °C (Figure 9). Peaks L + M represent pure helical (−g,−g) phosphates, while peaks J + K represent distorted helical conformations (deviations of dihedral angles of less than 60° from ±60° torsional angles). Apparently, ~12 phosphates are transferred from undistorted helical conformations to distorted helical conformations at higher temperature with $T_m \approx 58$–61 °C. At still higher temperature, peaks J + K gain a further 6 phosphates from the scattered peaks with the onset of secondary and tertiary structure melting. Both Sprinzl et al. (1974) and Hayashi et al. (1977) have also observed a cooperative conformational change of the molecule which occurs prior to the thermal denaturation transition.

$tRNA^{Phe}$ Melting in the Absence of Mg^{2+}. At lower temperature (<40 °C) the ^{31}P NMR spectra of $tRNA^{Phe}$ in the absence or in the presence of 10 mM Mg^{2+} are basically quite similar (Figures 1 and 3). Besides some shift differences (<0.6 ppm), the main difference between these spectra is a loss of intensity in the scattered peaks. The scattered signals B–F and S–U all integrate for less than 1 phosphate each at 36 °C, and excess intensity (5 phosphates) appears in the spectral region corresponding to nonhelical, "random coil" phosphates (−0.7 to 0 ppm; a shoulder to peak K). These spectral differences are largely due to partial melting of the native structure, as further shown by the changes in the ^{31}P spectra at higher temperature. Signal intensity for the main cluster shows a cooperative type of melting profile (Figure 5) similar to the 10 mM Mg^{2+} spectra, but the midpoint of the transition is 20 °C lower ($T_M \approx 48$ °C). This lowering is similar to melting transitions monitored by ^1H NMR (Kan

et al., 1977; Robillard et al., 1977). Little or no change in the chemical shifts of the scattered peaks occurs prior to their disappearance (between 41 and 51 °C). Some broadening of peaks B and C is observed between 41 and 46 °C with the line width for B increasing from 27 to 45 Hz and that for C from 15 to 33 Hz. As discussed earlier, this additional broadening with increasing temperature is due to chemical exchange between native and denatured structures. The 18-Hz chemical exchange broadening for B and C corresponds to a lifetime of ~18 ms.

Romer et al. (1969), Riesner et al. (1973), Urbanke et al. (1975), and Coutts et al. (1975) identified five different transitions in the thermal denaturation of tRNA^{Phe} in 30 mM Na^+ without added Mg^{2+} at pH 6.8, conditions comparable to our own. Transition 1 with $T_m \approx 25$ °C corresponds to melting of the tertiary structure (leaving the cloverleaf structure largely intact) and has a long lifetime of 10 ms (Romer et al., 1970). Transitions 2 and 3 with $T_m \approx 35$–40 °C and lifetimes of 2–23 and 17–475 ms (Coutts et al., 1975) correspond to melting of the remaining tertiary structure and the acceptor and anticodon stem hairpin loop structure (Figure 8). A fourth transition with a short (20–100 μs) lifetime and $T_m \approx 45$–50 °C corresponds to melting of the TψC loop, and a fifth transition with a similar lifetime and $T_m \approx 60$–65 °C corresponds to melting of the HU loop.

Since no scattered peaks are observed at temperatures greater than 50 °C and the TψC and HU hairpin loops are still largely unmelted[3] at this temperature, it is unlikely that the scattered peaks are assignable to TψC and HU loop secondary structures (and by inference not to the acceptor and anticodon loops as well). The earlier lifetime comparisons and these intensity changes thus suggest that *the scattered peaks originate from tertiary structure.*

Origin of Scattered Peaks. As discussed earlier, torsional effects can reasonably explain only ~2-ppm difference between the chemical shifts of unstrained phosphate diesters (Figure 7). The ~7-ppm range for the scattered diester peaks could be associated with bond angle deformation induced by tertiary interactions (Gorenstein, 1975, 1978). Four of these tertiary interactions are associated with intercalation between bases in different loops (Sussman et al., 1978). Patel (1974) has shown that intercalation of actinomycin D into a double helix can lead to ^{31}P downfield shifts of up to 2.9 ppm. It is certainly attractive to assign the downfield scattered B, C, D, and E peak signals to these intercalation tertiary interactions. Bond angle distortions from other tertiary interactions may also reasonably explain the upfield scattered peaks (increased bond angles).

One other tertiary interaction involving hydrogen bonding between the phosphate of residue 36 and the 2′-OH group of U_{33} is likely *not* responsible for the large shift of a scattered peak since we have previously found that hydrogen-bonding interactions in the binding of nucleotide monoesters to the positively charged active site of pancreatic RNase A lead to only small (<0.1 ppm) ^{31}P shifts (Gorenstein et al., 1976b).

^{31}P NMR provides the virtually unique ability to monitor the backbone conformation of tRNA and to monitor conformational transitions in this structure. Further efforts to assign the scattered peaks to individual phosphates will be rewarding and will provide a powerful probe of the solution conformation of this molecule.

[3] Between 51 and 71° the intensity of the non-g,g random coil peak increases by ~16 phosphates while that of the helical g,g phosphates decreases by the same amount (Figure 7). A total of 14 helical stem phosphates are in TψC and HU loops.

Acknowledgments

We acknowledge the contribution of Kenneth Kovar to a portion of this work. We also wish to show our appreciation to the Purdue Biological Magnetic Resonance Facility and to Dr. Jerry Dallas for his helpful comments.

References

Abragam, A. (1961) *The Principles of Nuclear Magnetism*, Oxford University Press, New York.
Berden, J. A., Cullis, P. R., Hoult, D. I., McLaughlin, A. C., Radda, G. K., & Richards, R. E. (1974) *FEBS Lett. 46*, 55.
Blackburn, G. M., Cohen, J. S., & Weatherall, I. (1971) *Tetrahedron 27*, 2903.
Bolton, P. H., & Kearns, D. R. (1977) *Biochemistry 16*, 5729.
Canet, D., Levy, G. C., & Peat, I. R. (1975) *J. Magn. Reson. 18*, 199.
Cole, P. E., & Crothers, D. M. (1972) *Biochemistry 11*, 4368.
Coutts, S. M., Riesner, D., Romer, R., Rabl, C. R., & Maass, G. (1975) *Biophys. Chem. 3*, 275.
Crothers, D. M., Cole, P. E., Hilbers, C. W., & Shulman, R. G. (1974) *J. Mol. Biol. 87*, 63.
Davanloo-Malherbe, P., Sprinzl, M., & Cramer, F. (1978) *Jerusalem Symp. Quantum Chem. Biochem. 11*, 125.
Freeman, R., & Hill, H. D. W. (1971) *J. Chem. Phys. 54*, 3367.
Gorenstein, D. G. (1975) *J. Am. Chem. Soc. 97*, 898.
Gorenstein, D. G. (1977) *J. Am. Chem. Soc. 99*, 2254.
Gorenstein, D. G. (1978) *Jerusalem Symp. Quantum Chem. Biochem. 11*, 1.
Gorenstein, D. G., & Kar, D. (1975) *Biochem. Biophys. Res. Commun. 65*, 1073.
Gorenstein, D. G., Findlay, J. B., Momii, R. K., Luxon, B. A., & Kar, D. (1976a) *Biochemistry 15*, 3796.
Gorenstein, D. G., Wyrwicz, A. M., & Bode, J. (1976b) *J. Am. Chem. Soc. 98*, 2308.
Gueron, M. (1971) *FEBS Lett. 19*, 264.
Gueron, M., & Shulman, R. G. (1975) *Proc. Natl. Acad. Sci. U.S.A. 72*, 3482.
Hayashi, F., Akasaka, K., & Hatano, H. (1977) *Biopolymers 16*, 655.
Jack, A., Ladner, J. E., & Klug, A. (1976) *J. Mol. Biol. 108*, 619.
Kan, L. S., Ts'o, P. O. P., Sprinzl, M., Haar, F. v. d., & Cramer, F. (1977) *Biochemistry 16*, 3143.
Komoroski, R. A., & Allerhand, A. (1972) *Proc. Natl. Acad. Sci. U.S.A. 69*, 1804.
Levy, G. C., & Nelson, G. L. (1972) *Carbon-13 Magnetic Resonance for Organic Chemists*, Chapter 4, Wiley-Interscience, New York.
Levy, G. C., & Peat, I. R. (1975) *J. Magn. Reson. 18*, 500.
Patel, D. J. (1974) *Biochemistry 13*, 2396, 2388.
Patel, D. J., & Canuel, L. (1976) *Proc. Natl. Acad. Sci. U.S.A. 73*, 674.
Pople, J., Schneider, W. G., & Bernstein, H. J. (1959) *High Resolution Nuclear Magnetic Resonance*, McGraw-Hill, New York.
Quigley, G. L., Wang, A. H. J., Seeman, N. C., Suddath, F. C., Rich, A., Sussman, J. L., & Kim, S. H. (1975) *Proc. Natl. Acad. Sci. U.S.A. 72*, 4866.
Riesner, D., Maass, G., Thiebe, R., Philippsen, P., & Zachau, H. G. (1973) *Eur. J. Biochem. 36*, 76.
Robillard, G. T., Tarr, C. E., Vosman, F., & Reid, B. R. (1977) *Biochemistry 16*, 5261.
Romer, R., Riesner, D., Maass, G., Wintermeyer, W., Thiebe,

R., & Zachau, H. G. (1969) *FEBS Lett. 5*, 15.
Romer, R., Riesner, D., & Maass, G. (1970) *FEBS Lett. 10*, 352.
Sprinzl, M., Kramer, E., & Stehlik, D. (1974) *Eur. J. Biochem. 49*, 595.
Stout, C. D., Mizuno, H., Rao, S. T., Swaminathan, P., Rubin, J., Brennan, T., & Sundaralingam, M. (1978) *Acta Crystallogr., Sect. B 34*, 1529.
Sundaralingam, M. (1969) *Biopolymers 7*, 821.
Sussman, J. L., Holbrook, S. R., Warrant, R. W., Church, G. M., & Kim, S. H. (1978) *J. Mol. Biol. 123*, 607.
Urbanke, C., Romer, R., & Maass, G. (1975) *Eur. J. Biochem. 55*, 439.
Valenik, A., & Lynden-Bell, R. M. (1970) *Mol. Phys. 19*, 371.
Weiner, L. M., Backer, J. M., & Rezvukhin, A. I. (1974) *FEBS Lett. 41*, 40.

Antibody–Nucleic Acid Complexes. Inhibition of Translation of Silkmoth Chorion Messenger Ribonucleic Acid with Antibodies Specific for 7-Methylguanosine†

Theodore W. Munns,* Charles S. Morrow, James R. Hunsley, Robert J. Oberst, and M. Kathryn Liszewski

ABSTRACT: Antibodies specific for 7-methylguanosine (m^7G) were evaluated for their ability to inhibit the translation of chorion mRNA in a wheat germ, cell-free amino acid incorporating system. Results obtained with antibody concentrations of 0.5–1.5 μM revealed dose-dependent inhibition of [^{3}H]-labeled amino acid incorporation into acid-insoluble radioactivity. Inhibition of translation was attributed to the interaction of anti-m^7G antibodies with the 5′ termini of chorion mRNAs on the basis that (a) anti-m^7G antibodies coupled to Sepharose (anti-m^7G–Sepharose) immunospecifically retained 5′-terminal cap structures of chorion mRNAs, i.e., m^7G (5′)ppp(5′)N^m, (b) significant inhibition of translation required a 2-h preincubation of anti-m^7G antibodies with mRNA, and (c) similar preincubation periods with anti-m^7G antibodies in the presence of the competing nucleoside hapten (m^7G) obviated the inhibitory effect of the antibody. The nature of the anti-m^7G antibody–mRNA complex was examined by digesting chorion mRNA with nuclease P_1 before (predigested) and after (postdigested) immunospecific adsorption to anti-m^7G–Sepharose adsorbent. Whereas predigested preparations yielded a single cap structure of the type m^7G(5′)ppp(5′)N, the predominating cap in the postdigested sample was m^7G(5′)ppp(5′)NpNpN. These latter data revealed that the nucleotide sequence adjacent to the cap was not significantly masked by the antibody and suggest the utility of anti-m^7G antibody as a site-specific probe.

The research described herein was prompted by numerous observations which have revealed the necessity of m^7G-containing[1] 5′-terminal oligonucleotide "caps" [m^7G(5′)-ppp(5′)N^m or m^7G(5′)ppp(5′)N^mpN^m] for the efficient in vitro translation of mRNAs (Shatkin, 1976; Revel & Groner, 1978). Initially, Both et al. (1975a,b) observed that the in vitro translation (wheat germ) of unmethylated, yet capped viral mRNA was significantly impaired when contrasted to control, m^7G-capped mRNA preparations. Decreased translational efficiencies were also observed with other mRNA preparations which had been chemically (Muthukrisnan et al., 1975; Kemper, 1976) or enzymatically (Shimotohno et al., 1977) treated for specific removal of the m^7G residue in their cap structures. The inability of these unmethylated or decapped mRNAs to interact with 40S ribosomal subunits further suggested that 5′-terminal caps provide a recognition signal for subsequent binding of mRNA to the ribosome (Both et al., 1975b), presumably by interacting with one or more initiation factors (Revel & Groner, 1978). Additional support for such a translational function has been provided by the finding that cap analogues inhibited the translation of capped mRNAs as well as their binding to ribosomes (Hickey et al., 1976; Weber et al., 1978). Controversy, however, persists as to the relative importance of the cap in translation. Thus, the degree of inhibition observed with uncapped mRNA or with cap analogues was found to be influenced by the concentrations of potassium ions (Weber et al., 1978; Chu & Rhoads, 1978) as well as the type of in vitro translational system employed (Lodish & Rose, 1977).

In view of the above and other findings which indicate the ability of selected antibody populations to immunospecifically recognize methylated nucleosides (Erlanger & Beiser, 1964; Levine et al., 1971; Munns et al., 1977a), we became interested in examining if antibodies specific for 7-methylguanosine (i.e., anti-m^7G antibodies) would inhibit the in vitro translation of chorion mRNA. Besides investigating the effects of anti-m^7G antibodies on in vitro translation, we conducted additional experiments to evaluate (a) the ability of anti-m^7G–Sepharose adsorbents to retain m^7G-containing caps derived from RNase T_2 digests of chorion mRNA and (b) the nature of the

† From The Edward A. Doisy Department of Biochemistry, Saint Louis University School of Medicine, St. Louis, Missouri 63104. *Received April 3, 1979.* This investigation was supported by National Cancer Institute Grant CA 17715 (T.W.M.) and National Institute of General Medical Sciences Grant GM 21961 (J.R.H.) awarded by the Department of Health, Education and Welfare.

[1] Abbreviations used: 7MeGua, m^7G, and pm^7G represent the base, nucleoside, and 5′-phosphate of 7-methylguanosine, respectively; 6MeAde, m^6A, and pm^6A represent the base, nucleoside, and 5′-phosphate of N^6-methyladenosine, respectively; 6,6Me_2Ade, N^6,N^6-dimethyladenine; N, nucleoside; N^m, 2′-*O*-methyl nucleoside; anti-m^7G antibody, anti-7-methylguanosine antibody; anti-m^7G–Sepharose, anti-m^7G antibody coupled to Sepharose; Cl_3AcOH, trichloroacetic acid; RNase, ribonuclease; $NaDodSO_4$, sodium dodecyl sulfate.

0006-2960/79/0418-3804$01.00/0